

# Design Analysis of a Magnetic Gear Box with Continuous Ratio Shifting

B. Majidi<sup>1\*</sup>, A. Baktash<sup>1</sup> and J. Milimonfared<sup>2</sup>

<sup>1</sup>Department of Electrical Engineering, Najafabad Branch, Islamic Azad University, Isfahan, Iran; bmx@aut.ac.ir

<sup>2</sup>Department of Electrical Engineering, Amirkabir University of Technology, Tehran - 15916, Iran

## Abstract

Magnetic gears offer important potential benefits compared with mechanical gears such as reduced maintenance, improved reliability, inherent overload protection, and physical isolation between the input and output shafts. This paper presents the theory and simulation results for a continuous magnetic gear box employed in wind generators, electric vehicles and other related applications in which continuous ratio of gear box is essential. The analysis is performed by Finite Element Method (FEM) to predict output torque, speed and magnetic field distribution inside the gear box. The gear box made up of an inner rotating part which is similar to the rotor of a 3 phase wound rotor induction motor and an outer rotating part which consists of 6 PM poles. Both the inner rotor and outer rotor can be exploited as a low/high speed rotating part. The output torque and other parameters are evaluated in steady state condition using vector analysis. Simulation results are in good agreement with theoretical analysis as well.

**Keywords:** Continuous, Finite Element Method (FEM), Magnetic Gear, Permanent Magnet

## 1. Introduction

Mechanical gear boxes are employed widely to transmit torque between separate parts moving at different speeds in various applications. For example they are used in wind power generators to increase the rotational speed and in electric ship propulsion to decrease the rotational speed. Because of their physical contact, mechanical loss, gear noise and regular lubrication are inevitable. In the last decade magnetic gear coupling has been proposed. Magnetic gears can transmit torque without mechanical contact. They are based on the same principle as the mechanical systems where the teeth are replaced by magnet pieces. They can transform torque and change speed by interactive magnetic field between the permanent magnet pieces<sup>1-3</sup>.

Magnetic gears offer substantial advantages compared to mechanical gears such as reduced maintenance, improved reliability, minimum acoustic noise, and inherent over load protection. At first because of the complicated structure, low efficiency and weak torque magnetic gears in

spite of some advantages have not gained much attention. In 2001 the Surface Permanent Magnet-type (SPM-type) magnetic gear was introduced in a practical application on account of its novel design<sup>4</sup>. Since then, various types of magnetic gears have been proposed to develop torque density, lower torque ripple, higher ratios and efficiency<sup>5-9</sup>. Recent efforts focus on implementing of continuous ratio to employed for wind generators, electric vehicles and other analogous applications in which continuous ratio of gear box is essential<sup>10-12</sup>. Reference<sup>13</sup> proposes a new magnetic gear based on super conductors to achieve high torque density. In 2004-2005 in linear motors field, linear-type magnetic gears were designed<sup>14</sup>. Reference<sup>15</sup> proposed a new design of cycloid-type magnetic gears to achieve more torque density at high ratio. References<sup>16-17</sup> proposed a new type of magnetic gear named axial-type magnetic gear. References<sup>18-19</sup> suggested a harmonic-type magnetic gear similar to harmonic mechanical gear. As the coaxial magnetic gears are the most applicable type of magnetic gears, the new arrangement of PMs is applied in this type of magnetic gears. One of the most popular arrangements is

\*Author for correspondence

Coaxial Magnetic Gear with Halbach Permanent-Magnet Arrays<sup>20-22</sup>. Recently, for implementing continuous ratio gear box, a structure has been devised which provide variable speed but has sophisticated structure<sup>23</sup>.

In this paper, continuous ratio capability and simple design for manufacturing are the main goals which are analyzed by Finite Element Method (FEM) and validated by vector analytical calculation. For predicting performance of the magnetic gear, the air-gap magnetic field is computed by steady state analytical method and would be compared with FEM results depicting air-gap magnetic field distribution. This adjustable continuous topology is quite suitable for many applications such as wind generators (which improves harmonic characteristics and eliminates back to back converters) and electric vehicles. This gear box can operate as a clutch and separate power from load. This advantage can make torque (speed) transmission systems very compact and simple. The operation principles of proposed magnetic gear box are presented first, and the design of this structure, which is consisted of the inner and the outer rotors is introduced, then. In the next step, the proposed gear box is mathematically analyzed and its descriptive equations are derived. Finally, the validity of the obtained formulas is confirmed by simulation of proposed structure in the Maxwell® software.

## 2. Principle of Operation

Figure 1 shows the structure of the proposed magnetic gear box. It consists of an inner rotor with three phase windings and an outer rotor which includes PMs. Each part is made up of a steel 1010, this steel has high saturation point (almost 1.8T) which is suitable for this application. In this system the inner rotor windings produce a rotating magnetic field with desired speed and as a result of its interaction with the outer rotor permanent magnets, outer rotor rotates. It is obvious that controlling the inner rotor current frequency controls the gear box ratio, which is the main idea of this paper. In other words  $N2 = N1 + Nf$  in

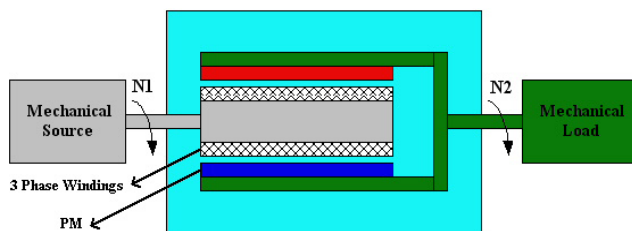


Figure 1. Proposed topology.

which  $N1$  is the mechanical speed of the inner rotor,  $Nf$  is the speed of the rotating magnetic field of the windings current frequency and  $N2$  is the speed of the outer rotor.

The purposed structure introduces various advantages:

- It is possible to use this topology as a high ratio gear box which is important in gear box applications.
- It is possible to use it as a speed regulator.
- Possibility of controlling the output torque.
- Inherent overload protection.
- The proposed topology can operate as a clutch and separate the prime-mover from load.
- Because of precision and high ratio of the proposed structure, it is possible to connect the generator output to the network (eliminating power electronic interfaces).
- Silent working.

## 3. Design of the Magnetic Gear Parts

### 3.1 Windings and slots of the inner rotor (Inner rotor)

One of the key parts of the proposed structure is the inner rotor which its design has a great impact on the performance and behavior of the whole system. The cogging torque of the magnetic gear box arises from the interaction of permanent magnets and the inner rotor slotted structure without the applied driving current<sup>24</sup>. Since an oscillatory torque always induces vibration, acoustic noise, and possible resonance especially at high load and low speed, the slots of the inner rotor have been designed in order to minimize the cogging torque. Figure 2 shows the structure of the inner rotor.

Windings type of the inner rotor is fractional slot and shorted pitch. This selection is based on evaluating of various windings performances in FEM simulation. This type of the inner rotor windings improves the machine

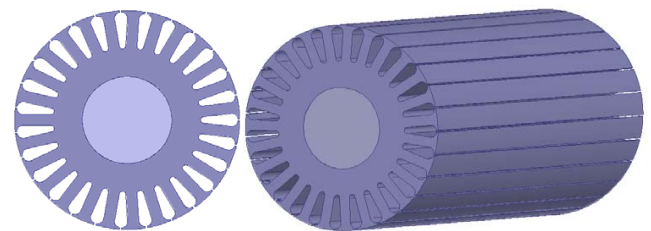


Figure 2. 2-3D view of the inner rotor.

characteristics such as harmonic specifications. With proper selection of windings step it is possible to minimize the attenuation coefficient for main frequency and maximize it for other harmonics. The inner rotor has 27 slots and its windings layout is according to Figure 3.

Parameters of the inner rotor windings are presented in Table 1. In this table  $q$  is the number of slots per pole per phase (spp),  $\gamma^{oe}$  is electrical step angle,  $K_d$  is distribution factor,  $K_p$  is shortage step coefficient of windings and  $\alpha$  is the slot angle.

The implemented and simulated models of the inner rotor are shown in Figure 4.

### 3.2 Outer Rotor

According to the inner rotor structure, the outer rotor designed and constructed which its model is shown in

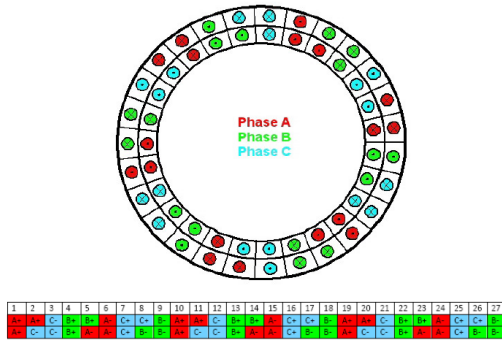


Figure 3. Windings layout in the inner rotor.

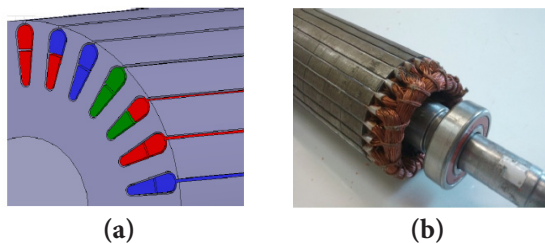


Figure 4. (a) Simulated model and (b) implemented view of the inner rotor.

Table 1. Inner rotor windings parameters

Parameter	Value
$q$ (spp)	1.5
$K_d$	0.9857
$K_p$	0.998
$\gamma$	30°
$\alpha$	13.33°

Figure 5. More details of the outer rotor design are discussed in part V. The permanent magnets are Neodymium rare earth type with grade of N35 (NdFe35).

## 4. Analysis of the Proposed Gear Box

The aim of this section is calculation of the output torque of the proposed gear box which is produced by interaction of two magnetic fields, one by windings current (in the inner rotor) and the other one by permanent magnets (in the outer rotor).  $F_{ri}$  is the peak value of the inner rotor windings Magneto Motive Force (MMF) and  $F_{ro}$  is the peak value of the outer rotor MMF. It is obvious that output torque is equivalent of the multiplex of these fields and sinus of the angle between them as shown in Fig. 6. For calculating output torque the following assumptions has been taken into account:

- The inner and outer rotors are made of material with infinite permeability
- Air gap length is much less than average radius, there is no difference in the inner rotor surface flux with the outer rotor surface flux.
- Only the main field component of the inner and outer rotors will be taken into account.

Magnitude of the resultant MMF in the air gap can be calculated as:

$$F_R = \sqrt{F_{ro}^2 + F_{ri}^2 + 2F_{ro}F_{ri} \cos \theta} \tag{1}$$

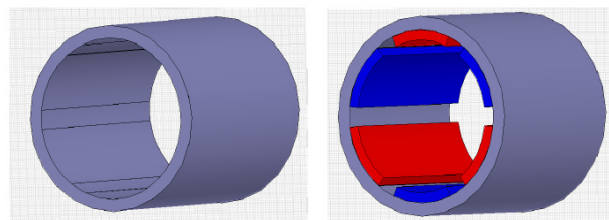


Figure 5. Simulated model of the outer rotor.

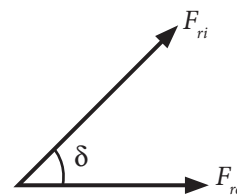


Figure 6. Field vectors of the inner and outer rotors.

The magnetic field intensity in the air gap  $H_g$  is:

$$H_g = \frac{F_R}{g} \quad (2)$$

Then the average of co-energy density in the air gap is:

$$W'_{fld} = \frac{1}{2} \frac{\mu_0}{g^2} \times \left( \frac{1}{2} F_R^2 \right) = \frac{1}{4} \mu_0 \left( \frac{F_R}{g} \right)^2 \quad (3)$$

Equations (1) and (3) can be combined to calculate the total co-energy in the air gap:

$$W'_{fld} = \frac{1}{2} \frac{\mu_0}{g^2} F_R^2 (2\pi r l g) = \frac{1}{2} \frac{\mu_0 \pi r l}{g} F_R^2 \quad (4)$$

$$W'_{fld} = \frac{1}{2} \frac{\mu_0 \pi r l}{g} (F_{ro}^2 + F_{ri}^2 + 2F_{ro} F_{ri} \cos \theta) \quad (5)$$

Considering  $\theta = \frac{P}{2} \theta_m$  the output torque can be written as:

$$T_e = \frac{\partial W'_{fld}}{\partial \theta_m} (F_{ro}, F_{ri}, \theta) = \frac{\partial W'_{fld}}{\partial \theta} (F_{ro}, F_{ri}, \theta) \frac{\partial \theta}{\partial \theta_m} \quad (6)$$

$$T_e = \frac{P}{2} \frac{\mu_0 \pi r l}{g} \frac{\partial}{\partial \theta} (F_{ro}^2 + F_{ri}^2 + 2F_{ro} F_{ri} \cos \theta) = -\frac{P}{2} \frac{\mu_0 \pi r l}{g} F_{ro} F_{ri} \sin \theta \quad (7)$$

Rewriting this equation with  $F_R$ :

$$T_e = -\frac{P}{2} \frac{\mu_0 \pi r l}{g} F_{ri} F_R \sin \delta \quad (8)$$

By substituting:

$$F_R = g \cdot H_p = g \cdot \frac{B_p}{\mu_0} \quad (9)$$

$$\phi = \frac{4}{P} B_p l r \rightarrow B_p = \frac{P}{4} \frac{\phi}{l r} \quad (10)$$

$$F_{ri} = m \frac{2\sqrt{2}}{\pi} k_w \frac{N_{ph} I}{P} \quad (11)$$

$$\phi = \frac{E_{ph}}{\sqrt{2\pi f N_{ph} k_w}} \quad (12)$$

Into Equation (8) it is possible to write it in a more useful form:

$$T_e = \frac{\pi}{8} P^2 \phi F_{ri} \sin \delta = -\frac{\pi}{8} P^2 \left( \frac{E_{ph}}{\sqrt{2\pi f N_{ph} k_w}} \right) \left( m \frac{2\sqrt{2}}{\pi} k_w \frac{N_{ph} I}{P} \right) \sin \delta \quad (13)$$

$$\sin \delta = \frac{P}{4\pi f} m E_{ph} I \sin \delta = \frac{1}{\omega_m} m E_{ph} I \sin \delta$$

In these equations  $\phi$  is the air gap flux,  $E_{ph}$  is induced voltage per phase in the inner rotor,  $N_{ph}$  is effective turns of the inner rotor windings per phase,  $K_w$  is the inner rotor windings coefficient and  $I$  is its current. Equation (13) can be written as in below:

$$T_e = \frac{1}{\omega_m} m E_{ph} I \sin \delta = \frac{1}{\omega_m} m E_{ph} I \cos \theta \quad (14)$$

Where,  $\delta = \theta + 90$  in which  $\theta$  is the phase angle between  $E_{ph}$  and  $I$ .

## 5. Simulation and Evaluation of the Proposed Gear Box

Herein, the design of the proposed magnetic gear and the associated points are presented and discussed, as well as evaluated based on the earlier-discussed issues. Table 2 summarizes the parameters of the devices.

It is worth noting that PM specifications cannot be chosen freely, and must be selected among the standard ones given in Table 3.

B-H characteristic of the utilized steel (M19) is depicted in Figure 7.

According to the mechanical considerations, the minimum air-gap length is chosen to be 0.8 mm as given in Table 2. The shaft radius also satisfies and provides us the torque transfer capability of 39 N.m. A satisfactory PM ratio of 0.7 is assigned so that the torque pulsations and back-EMF harmonics are simultaneously minimized, and the leakage flux will be limited. A 2-Dimensional Time-Stepping Finite Element Method (2-D TSFEM),

**Table 2.** Specifications of a proposed gear box

Parameter	Value	Parameter	Value
Shaft radius, $R_{sh}$	15 mm	axial length, $L$	140 mm
PM height, $h_{pm}$	5 mm	Number of PMs, $N_{pm}$	6
air-gap, $g$	0.8 mm	PM ratio, $a_m$	0.7
inner-rotor back-iron length, $L_{r,in}$	35.2 mm	steel grade	M19
outer-rotor back-iron length, $L_{r,out}$	10 mm	No. of inner-rotor slots	27
Turns per slot layer	33	Windings type	Fractional slot, fractional pitch,
Current density	5 A/mm <sup>2</sup>	Slot per pole per phase	1.5

**Table 3.** Specifications of standard PMs

Type	$B_r$ (T)	$H_c$ (kA/m)	Type	$B_r$ (T)	$H_c$ (kA/m)
N27	≈ 1.05	≈ 800	N40	≈ 1.27	≈ 928
N30	≈ 1.10	≈ 800	N42	≈ 1.30	≈ 928
N33	≈ 1.15	≈ 840	N45	≈ 1.35	≈ 870
N35	≈ 1.19	≈ 872	N48	≈ 1.40	≈ 840
N38	≈ 1.23	≈ 904	N50	≈ 1.42	≈ 840

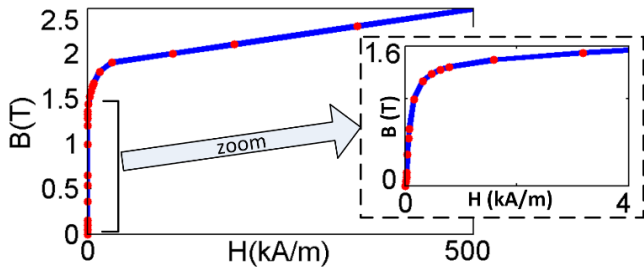


**Figure 7.** B-H characteristic of the utilized steel with grade M19-29G.

that its meshed regions is shown in Figure 8, is employed to evaluate the design outcomes. It should be mentioned that the mesh size shall be selected properly to achieve accurate results.

The proposed design also provides an appreciable demagnetization withstand capability by an appropriate field intensity ratio of  $H_m/H_c = 0.5$ . The Magnetic field intensity distribution within PMs shown in Figure 9, confirms the previous discussion as well, wherein it is seen that the armatures reaction fields under load condition do not have an influential demagnetization effect on PMs.

The rotor radius is large enough to avoid saturation and the length of the outer-rotor back iron is properly designed as well. The magnetic flux density distribution within the device is shown in Figure 10, validate the design.

This model has been used for various operating conditions to evaluate the proposed gear box behavior.

### 5.1 Generator Mode

Herein, if the outer rotor rotates at the speed of 1000 rpm while the inner rotor is fixed, the three phase voltage induced in the windings is determined as shown in Figure 11. It is seen that the voltage waveforms are sinusoidal that finally simplifies the drive system, all of which originates from the proper machine design, e.g. the inner-rotor windings and slots, and PMs.

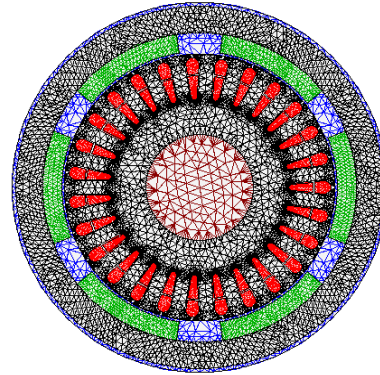


**Figure 8.** Meshed regions of the FEM employed for evaluating the proposed magnetic gear.

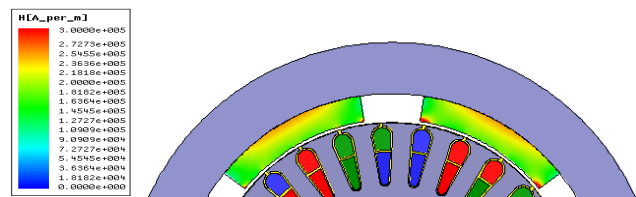


**Figure 9.** Magnetic field intensity distribution within PMs.

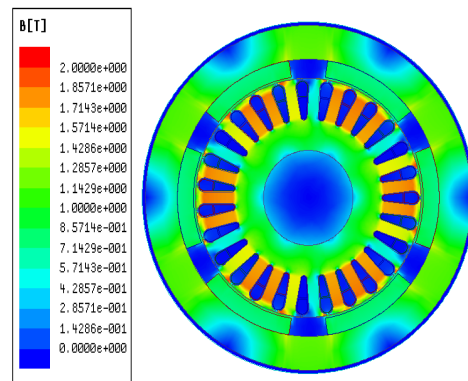


**Figure 10.** Magnetic flux density distribution within the proposed gear box.

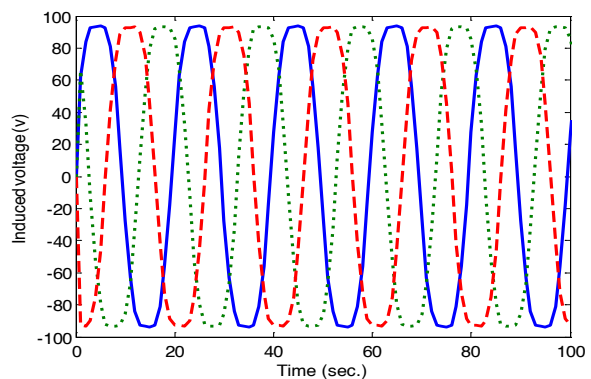


**Figure 11.** Induced voltage in the inner rotor windings.

### 5.2 Motor Mode

Before testing the proposed gear box it is necessary to obtain the output torque characteristic in the motor mode. The inner rotor is fixed and the outer rotor is rotated for 5 degrees until 200 degrees and the corresponding output torque is recorded for each step. Figure 12 shows the output torque versus the inner rotor positions. It can be seen that the maximum output torque is around 35N.m.

### 5.3 Gear Box Mode

In Figure 13, gear box torque and speed with 20 N.m loading are shown. Since the windings current frequency is 50Hz the rotating magnetic field is 1000 rpm, and the initial mechanical speed of the inner rotor is 500 rpm, therefore the speed of the outer rotor is 1500 rpm, i.e. 1000+500 rpm. It is observed that the gear box has been stabilized in desired values. Since in the generator mode the back-EMF amplitude was 96 volt, while the applied voltage is on the inner rotor terminals, to compensate for the voltage drop on the windings, the applied voltage is set to  $V_{peak} = 105$  volt, i.e. a little higher.

At this point, by simulating the motor mode without the outer rotor permanent magnets, it is possible to plot the air gap flux density and flux linkage waveforms (Figure 14) and evaluate equations (10) and (12).

Issued from the machine having the specifications given in Table 2, we achieve:  $\phi = 0.000442wb$ ,  $\lambda = 0.129wb$

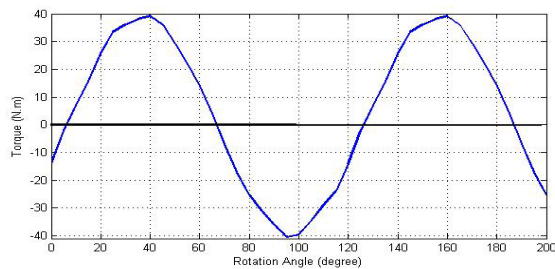


Figure 12. Torque versus rotor position.

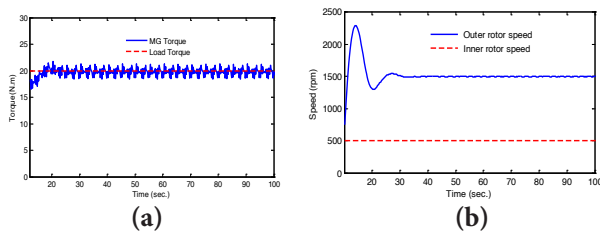


Figure 13. (a) Output torque and (b) speed of gear box in motor mode.

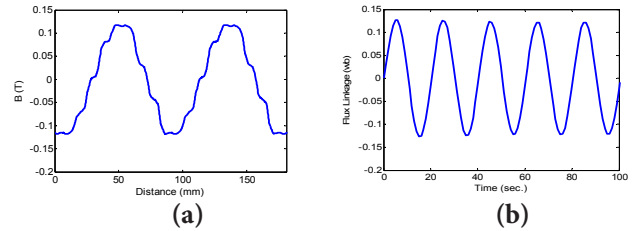


Figure 14. (a) Flux density and (b) flux linkage waveforms in the air gap caused by the inner rotor windings.

and the air gap flux density is  $B = 0.121$  T. Finally, by knowing the phase difference between voltage and current in the inner rotor windings, an output torque of 20.84 N.m is obtained. It is worth noting that the presented equations well describe the gear box behavior in steady state operation, and are in good agreement with those extracted from simulations.

## 6. Conclusion

In this paper, the analysis and simulation of a continuous magnetic gear box is carried out which can be employed in wind generators, electric vehicles, etc. wherein a continuous ratio of gear box is required. To this end, finite elements analyses are performed to predict the main characteristics of the device including output torque, speed and magnetic field distributions. Both the inner and the outer rotors can be exploited as a low/high speed rotating part by controlling the frequency of the inner rotor windings current. The output torque and other parameters are evaluated in the steady state condition using vector analysis. Simulation results are also in good agreement with theoretical analysis.

## 7. References

1. Tsurumoto K, Kikushi S. A new magnetic gear using permanent magnet. IEEE Trans Magn. 1987; 23(5):3622–4.
2. Huang DR, Yao YD, Lin SM, Wang SJ. The Radial Magnetic Couplings between Magnetic Gears. IEEE Trans Magn. 1995 Nov; 31(6):2317–21.
3. Yao YD, Huang DH, Lin SM, Wang SJ. Theoretical Computations of the Magnetic Coupling between Magnetic Gears. IEEE Trans Magn. 1996 May; 32(3):710–3.
4. Atallah K, Howe D. A novel high-performance magnetic gear. IEEE Trans Magn. 2001 Jul; 37(4):2844–6.
5. Rasmussen PO, Andersen TO, Jorgensen FT, Nielsen O. Development of a high-performance magnetic gear. IEEE Trans Ind Appl. 2005 May/June; 41(3):764–70.

6. Huang C, Tsai M, Dorrell DG, Lin B. Development of a magnetic planetary gearbox. *IEEE Trans Magn.* 2008 Mar; 44(3):403–12.
7. Bharathi Sankar A, Seyezhai R. Development of active neutral point clamped multilevel inverter fed BLDC drive employing FPGA. *Indian Journal of Science and Technology.* 2015 Feb; 8(4):392–9.
8. Niguchi N, Hirata K. Torque-speed characteristics analysis of a magnetic-gear motor using finite element method coupled with vector control. *IEEE Trans Magn.* 2013; 49(5):2401–4.
9. Rasmussen PO, Frandsen TV, Jensen KK, Jessen K. Experimental evaluation of a motor-integrated permanent-magnet gear. *IEEE Trans Ind Appl.* 2013; 49(2):850–9.
10. Sadeghi M, Gholami M. Fuzzy logic approach in controlling the grid interactive inverters of wind turbines. *Indian Journal of Science and Technology.* 2014 Aug; 7(8):1196–200.
11. Batra D, Sharma S, Ratan R. Axis Controlled Movement of Robot Using Brushless DC Motor Drive. *Indian Journal of Science and Technology.* 2009 Apr; 2(4):1196–200.
12. Elavarasi R, SenthilKumar PK. An FPGA based regenerative braking system of electric vehicle driven by BLDC motor. *Indian Journal of Science and Technology.* 2014 Nov; 7(7):1–5.
13. Okano M, Tsurumoto K, Togo S, Tamada N, Fuchino S. Characteristics of the magnetic gear using a bulk high-Tc superconductor. *IEEE Trans Appl Supercond.* 2002 Mar; 12(1):979–83.
14. Atallah K, Wang J, Howe D. A high-performance linear magnetic gear. *J Appl Phys.* 2005; 97:10N516-1–3.
15. Jorgensen FT, Andersen TO, Rasmussen PO. The Cycloid Permanent Magnetic Gear. *IEEE Trans Ind Appl.* 2008 Nov; 44(6):1659–65.
16. Mezani S, Atallah K, Howe D. A high-performance axial-field magnetic gear. *J Appl Phys.* 2006; 99:08R303-1–3.
17. Acharya VM, Bird JZ, Calvin M. A flux focusing axial magnetic gear. *IEEE Trans Magn.* 2013; 49(7):4092–5.
18. Rens J, Clark R, Calverley S, Atallah K, Howe D. Design, analysis and realization of a novel magnetic harmonic gear. 18th International Conference on Electrical Machines (ICEM). 2009. p. 1–4.
19. Rens J, Atallah K, Calverley SD, Howe D. A novel magnetic harmonic gear. *IEEE Trans Ind Appl.* 2010 Jan/Feb; 46(1):206–12.
20. Zhu ZQ, Howe D. Halbach permanent magnet machines and applications: A review. *Inst Electr Eng Proc Electr Power Appl.* 2001 Jul; 148(4):299–308.
21. Choi J, Yoo J. Design of a Halbach magnet array based on optimization techniques. *IEEE Trans Magn.* 2008 Oct; 44(10):2361–6.
22. Jian L, Chau KT. A Coaxial Magnetic Gear With Halbach Permanent-Magnet Arrays. *IEEE Trans Energy Convers.* 2010 Jun; 25(2):319–28.
23. Shah L, Cruden A, Williams BW. A variable speed magnetic gear box using contra-rotating input shafts. *IEEE Trans Magn.* 2011 Feb; 47(2):431–8.
24. Niguchi N, Hirata K. Cogging Torque Analysis of Magnetic Gear. *IEEE Trans Ind Electron.* 2012; 59(5):2189–97.